

YOUNG ENERGETIC PSR J1617–5055, ITS UNDERLUMINOUS NEBULA AND UNIDENTIFIED TEV SOURCE HESS J1616–508

O. KARGALTSEV^{1,2}, G. G. PAVLOV², AND J. A. WONG²

Draft version October 28, 2018

ABSTRACT

We observed the young energetic pulsar J1617–5055 with the *Chandra* ACIS detector for 60 ks. In addition to the pulsar, the X-ray images show a faint pulsar-wind nebula (PWN) seen up to $\sim 1'$ from the pulsar. Deconvolution and reconstruction of the image reveal a brighter compact PWN component of $\sim 1''$ size, possibly with a jet-torus morphology. The PWN spectrum fits an absorbed power-law (PL) model with the photon index $\Gamma \approx 1.5$. The total PWN luminosity in the 0.5–8 keV band, $L_{\text{pwn}} = 3.2 \times 10^{33}$ ergs s^{-1} for $d = 6.5$ kpc, is a fraction of 2×10^{-4} of the pulsar's spin-down power \dot{E} and a fraction of 0.2 of the pulsar's X-ray luminosity, which is a factor of 20 lower than one would expect from an average empirical relation found for a sample of PWNe observed with *Chandra*. The pulsar's spectrum can be described by an absorbed PL with $n_H \approx 3.5 \times 10^{22}$ cm^{-2} and $\Gamma \approx 1.1$, harder than any other pulsar spectrum reliably measured in the soft X-ray band. This non-thermal emission is $\approx 50\%$ pulsed showing one peak per period. We have also investigated a possible connection between J1617 and the extended TeV source HESS J1616–508 whose center is located $10'$ west of the pulsar. We find no preferential extension of the X-ray PWN toward the TeV source. Therefore, the *Chandra* data do not provide conclusive evidence for PSR J1617–5055 and HESS J1616–508 association. We have also analyzed archival X-ray, radio, and IR data on the HESS J1616–508 region and found traces of diffuse emission (resembling a shell in the radio) coinciding with the central part of HESS J1616–508. We speculate that the TeV source may be multiple, with most of the emission coming from an unknown SNR or a star-forming region, while some fraction of the TeV emission still may be attributed to the J1617 PWN.

Subject headings: ISM: individual (HESS J1616–508) — pulsars: individual (PSR J1617–5055) — stars: neutron — X-rays: ISM

1. INTRODUCTION

High-resolution X-ray observations of young ($\tau \lesssim 10$ kyrs) rotation-powered pulsars usually show a pointlike pulsar embedded in a pulsar wind nebula (PWN). In most cases, the pulsar emission is dominated by the nonthermal emission generated in the pulsar magnetosphere. The X-ray spectrum of this emission usually fits power-law model with typical photon indices $\Gamma \simeq 1$ –2. As a rule, the nonthermal emission component is strongly pulsed, showing one or more peaks per period. Studying the non-thermal emission constrains the emission and particle acceleration mechanisms in the pulsar magnetosphere. Young pulsars are also interesting because they emit strong magnetized relativistic winds which interact with the ambient medium and form PWNe whose emission is interpreted as synchrotron radiation from the shocked pulsar wind (see Kaspi et al. 2006; Gaensler & Slane 2006; Kargaltsev & Pavlov 2008, hereafter KP08, for reviews). Studying PWNe helps to understand the structure and dynamics of relativistic pulsar winds, elucidate the mechanisms of PWN formation, evolution and interaction with the ambient medium, and establish the properties of the relativistic plasma in PWNe.

The young ($\tau \equiv P/2\dot{P} = 8.13$ kyr; $\dot{E} = 1.6 \times 10^{37}$ ergs s^{-1}) 69 ms pulsar J1617–5055 (hereafter J1617) was first identified through its X-ray pulsations with *ASCA* (Torii et al. 1998)³ with the radio pulsations found shortly afterwards (Kaspi et

al. 1998). The *ASCA* spectrum of the pulsar was described by the absorbed power-law (PL) model with the photon index $\Gamma = 1.4 \pm 0.2$ and observed flux $F_X = (3.6 \pm 0.2) \times 10^{-12}$ ergs $\text{s}^{-1} \text{cm}^{-2}$ in the 3–10 keV band (Torii et al. 2000).

Since the *ASCA* detection, J1617 has been observed with other X-ray satellites. It was imaged $6'$ off-axis in *Chandra* ACIS observations of the RCW 103 supernova remnant (SNR) in 1999 September (Garmire et al. 1999) and February 2000. It was also observed by *XMM-Newton* in 2001 September (two pointings, 30 ks aimed at the pulsar, and 20 ks centered at RCW 103). The J1617 properties inferred from these *XMM-Newton* observations have been briefly reported by Becker & Aschenbach (2002; hereafter BA02). They found that the spectrum in the 0.5–10 keV band fits the absorbed PL model with $\Gamma = 1.1$ –1.4, $n_H = (2.8$ – $3.6) \times 10^{22}$ cm^{-2} , and unabsorbed flux $F_X^{\text{unabs}} = (4.9$ – $5.4) \times 10^{-12}$ ergs $\text{s}^{-1} \text{cm}^{-2}$ (the numbers correspond to the 90% confidence range). BA02 have also detected pulsations with a single, asymmetric pulse and a pulsed fraction of $\sim 50\%$ in the 2.5–15 keV band. These observations confirmed the non-thermal nature of the pulsar emission; however, they lacked the resolution needed to separate the pulsar emission from the emission of a possible compact PWN around this young, remote pulsar. J1617 was also observed serendipitously by *XMM-Newton* in 2005 August (≈ 90 ks).

J1617 has been also detected at higher energies with *RXTE* PCA/HEXTE (2–60 keV band; Torii et al. 2000; Kuiper 2007), and *Integral* IBIS/ISGRI (20–300 keV band; Landi et al. 2007). Landi et al. (2007) have produced a joined spectral fit to the *XMM-Newton*, *BeppoSAX*, and *Integral* data and found fitting parameters close to those obtained by BA02 from the *XMM-Newton* data alone [$\Gamma = 1.4 \pm 0.1$,

¹ Dept. of Astronomy, University of Florida, Bryant Space Science Center, Gainesville, FL 32611; oyk100@astro.ufl.edu

² The Pennsylvania State University, 525 Davey Lab, University Park, PA 16802, USA; pavlov@astro.psu.edu

³ The 69 ms pulsations from this region were first detected with *Ginga* (Aoki et al. 1992), but it was impossible to determine the source of these pulsations because of the very poor angular resolution of *Ginga*.

$n_H = (3.9 \pm 0.3) \times 10^{22} \text{ cm}^{-2}$, and $F_X^{\text{unabs}} = 4.2 \times 10^{-12} \text{ ergs cm}^{-2} \text{ s}^{-1}$ in 2–10 keV]. Fitting the *RXTE* spectrum in the 2–30 keV band with a power-law model, Kuiper (2007) found $\Gamma = 1.30 \pm 0.01$ for fixed $n_H = 3.2 \times 10^{22} \text{ cm}^{-2}$.

Observations of J1617 and its surroundings have become particularly interesting after the discovery of the extended ($\sim 20'$ in diameter) TeV source HESS J1616–508 (hereafter HESS J1616) by Aharonian et al. (2006). Although its center of gravity is offset by $\approx 10' - 11'$ from the pulsar, the extent of the TeV emission still encompasses the pulsar location. The HESS J1616 spectrum above 200 GeV fits a power-law model with $\Gamma = 2.35 \pm 0.06$ and 1–10 TeV flux $F_{\text{TeV}} \approx 1.7 \times 10^{-11} \text{ ergs s}^{-1} \text{ cm}^{-2}$. The central region of HESS J1616 was observed with *Suzaku* XIS, but no X-ray counterpart was found to a limiting flux of $3.1 \times 10^{-13} \text{ ergs cm}^{-2} \text{ s}^{-1}$, so that the TeV source was suggested to be “the best example in the Galaxy of a dark particle accelerator” (Matsumoto et al. 2007). Landi et al. (2007) observed the field of HESS J1616 with *Integral* IBIS/ISGRI and *Swift* XRT, and also analyzed archival *XMM-Newton* and *BeppoSAX* data. These authors concluded that J1617 is the only plausible counterpart to the TeV source.

For many young pulsars, radio or X-ray SNR associations have been found, but no SNR association has been established for J1617 so far. Although J1617 is just $\sim 7'$ north of the center of the RCW 103 SNR, outside of the $5'$ SNR radius, the pulsar is almost certainly unrelated to the SNR. RCW 103 hosts a central compact object (CCO; possibly a NS binary or a transient magnetar; e.g., Pavlov et al. 2002, 2004; de Luca et al. 2007), which is a more plausible candidate for the compact remnant of the SN explosion. In addition, the RCW 103 spectrum shows a significantly smaller interstellar absorption than J1617 (Gotthelf et al. 1997). The relative positions and sizes of HESS J1616 and RCW 103 suggest that the HESS source is also not associated with the SNR.

To search for a compact X-ray PWN around J1617 and separate the pulsar and PWN emission, we have carried out a deep *Chandra* ACIS observation of J1617 in 2006 June, with the pulsar placed near the optical axis. Here we report the results of this observation and our analysis of archival multiwavelength data on J1617 and HESS J1616. In §2 we describe the observations, the images of the J1617 PWN and the HESS J1616 field, and the spectral analysis of the pulsar and the PWN. We discuss the pulsar and PWN properties and the nature of HESS J1616 in §3, and summarize our findings in §4.

2. OBSERVATIONS AND DATA ANALYSIS

We observed J1617 with the *Chandra* ACIS detector on 2006 June 6 (ObsID 6684) for 60 ks in Timed Exposure (TE) mode with Very Faint (VF) telemetry format. The pulsar was imaged on the ACIS-I3 chip near the optical axis. The other ACIS chips were turned off. To reduce the pile-up in the pulsar image, we used 1/4 subarray ($\approx 8' \times 2'$ field of view [FOV]; frame time 0.84104 s, including 0.8 s exposure time and 0.04104 s “dead time”). No substantial background changes were detected during the entire observation. The scientific exposure time was 57.24 ks.

We will also use in this work two archival *Chandra* ACIS imaging observations of 1999 September 26 (ObsID 123) and 2000 February 8 (970). As the primary target of those observations was the RCW 103 SNR, the pulsar was imaged $\approx 6'$ off-axis, which resulted in a broadened point spread function (PSF). The frame time was 3.24104 s in both observations

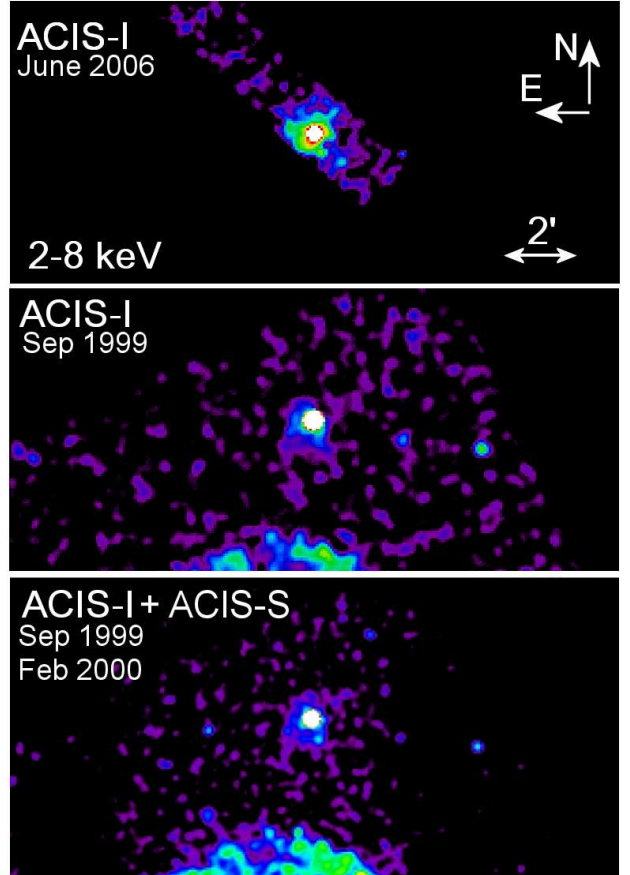


FIG. 1.— *Chandra* images of the field around J1617 with the observation dates listed in the images (see Table 1 for details). The *bottom* panel shows the combined image from 1999 and 2000 observations. All the images are binned to a pixel size of $4''$ and then smoothed with the $r = 12''$ gaussian kernel. The contrast is chosen to emphasize the faint large-scale emission. The extended shell, partly seen in the *middle* and *bottom* images, belongs to RCW 103.

(other details are given in Table 1.) The second observation suffered from significant background flares (up to 6 times the quiescent level). Filtering out the flares reduced the exposure by ≈ 5 ks.

In addition we analyzed the ACIS observation of 2002 March 3 (ObsID 2759). The data were taken in Continuous Clocking (CC) mode, which allows one to achieve time resolution of 2.85 ms at the expense of spatial information in one dimension.

The central part of HESS 1616 was serendipitously imaged on the ACIS S2 and S3 chips during the *Chandra* observations of the Kes 32 SNR that occurred on 2001 October 10 (ObsID 1960). The data were taken in Faint Mode, and the scientific exposure time was 29 ks (Vink 2004).

Reduction of the *Chandra* data was done with the *Chandra* Interactive Analysis Observations (CIAO) software (ver. 3.4, 4.0; CALDB ver. 3.3.0.1, 3.4.0) and FTOOLS (ver. 6.3). In our image analysis we have made use of MARX⁴ and *Chandra* Ray Tracer (ChaRT) software⁵. We also used XSPEC (ver. 11.3.2) for the spectral analysis.

J1617 was first observed with the *XMM-Newton* EPIC MOS1 and MOS2 detectors on 2001 September 9 (ObsID

⁴ MARX (Model of AXAF Response to X-rays) is a suite of programs designed to enable the user to simulate the on-orbit performance of the *Chandra* satellite. See <http://space.mit.edu/ASC/MARX/>

⁵ The software is available at <http://cxc.harvard.edu/chart/>.

TABLE 1
CHANDRA OBSERVATIONS OF J1617.

ObsID	123	970	2759	6684
Date	1999 Sep 26	2000 Feb 8	2002 March 03	2006 June 6
Mode, chip region	TE, Full Frame	TE, Full Frame	CC, Full Frame	TE, 1/4-subarray
Telemetry format	VF	F	F	VF
Chips activated	I0-I3, S2,S3	I2,I3,S2-S4	I2,I3,S1-S4	I3
J1617 imaged on	I1	I3	S2	I3
Off-axis angle	6.1'	6.1'	6.3'	40''
Sci. Exp., ks	13.92	13.75	48.82	57.24

NOTE. — Except for ObsID 970, the scientific exposures coincide with the live times given in the EVT2 file headers (for the chip of interest). In ObsID 970, removing the flares reduced this time by ≈ 5 ks.

TABLE 2
COUNT STATISTICS FOR THE SPECTRAL EXTRACTION REGIONS

Region	A	N_{tot}	N_{bg}	N_{src}	S/N	\mathcal{S}
inner PWN	3.14	1162 ± 32	732 ± 75	430 ± 82	5.2	2.39 ± 0.46
outer PWN	2610	959 ± 31	445 ± 21	514 ± 37	13.9	$(3.44 \pm 0.25) \times 10^{-3}$

NOTE. — Source (N_{src}), total (N_{tot}) and background (N_{bg}) counts are extracted from the regions with an area A (in arcsec²) shown in Figures 2 and 4, in the 0.5–8 keV band. For *inner* PWN the uncertainty of the background, $\simeq 10\%$, is mostly systematic (due to the uncertainties involved in the PSF simulation). The mean surface brightness \mathcal{S} is in units of counts ks⁻¹ arcsec⁻² in the 0.5–8 keV band.

0113050701)⁶. J1617 was also serendipitously observed with the same detectors during the observation of RCW 103 on 2005 August 23 and 24 (ObsID 0302390101). In both observations the two MOS cameras were operated in Full Window mode (2.6 s time resolution) with the Medium optical filter; the dead-time corrected exposure times were ≈ 28 and ≈ 86 ks. During the 2001 observation, the EPIC PN camera was in Timing mode, while it was in Small Window mode, with J1617 outside of the FOV, during the 2005 observation. For the *XMM-Newton* data analysis, we used the Processing Pipeline Subsystem (PPS). Both the 2001 and 2005 observations were strongly contaminated by flares during which the background count rate exceeded the quiescent level by a factor of up to 16. Filtering the flares out left 22.2 ks and 70.3 ks useful scientific exposure for the first and second observations respectively.

2.1. PWN and pulsar images

Figure 1 shows binned and smoothed large-scale images of J1617 and its surroundings in the 2–8 keV band. The upper panel shows the 1/4 subarray ACIS-I3 image from our observation of 2006 June. In this image we see a relatively bright pointlike source at the radio pulsar position embedded in faint diffuse emission more extended toward south and southeast of the pulsar. The asymmetry is better seen in the ACIS images from earlier observations (Fig. 1, *middle* and *bottom*), which have larger FOVs, with the pulsar $\approx 3'$ north of the RCW 103 shell seen near the bottom in each of the two images.

Figure 2 shows a close-up view of J1617 and its immediate vicinity from our observation of 2006 June. With the pulsar imaged on-axis, this observation provides a much better resolution than the off-axis ACIS observations of 1999 and 2000.

⁶ J1617 was also serendipitously imaged off-axis in the observation 0113050601 on the same date. We do not analyze this observation because a much longer *XMM-Newton* observation of 2005 August is available, with the about the same pointing and roll angle.

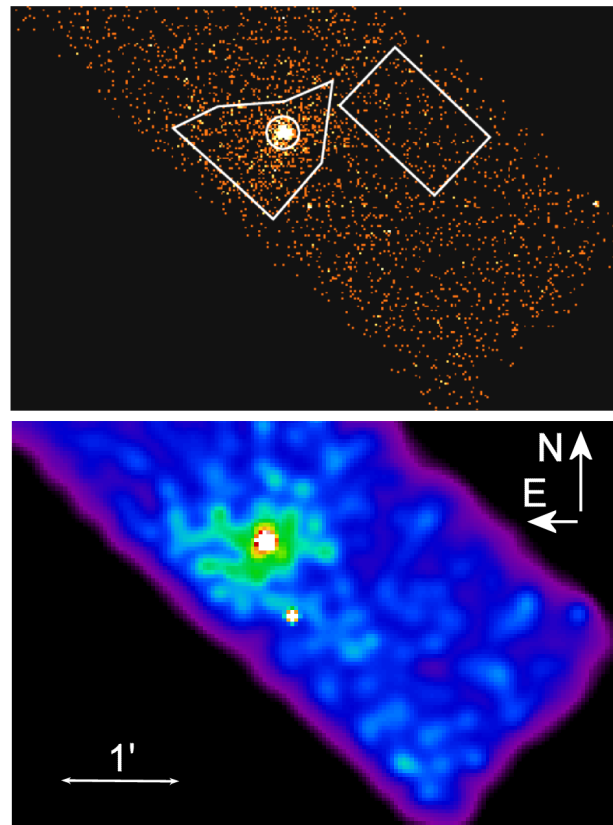


FIG. 2.— ACIS-I3 (1/4 subarray) image of J1617 and its vicinity in the 2–8 keV band, binned by a factor of 2 (pixel size 0.98''). *Top*: Unsmoothed image with the regions used for extraction of the extended PWN spectrum (within the polygon, excluding the circle; see §2.3.2 and Tables 2 and 3) and the background (box). *Bottom*: The same image adaptively smoothed with *csmooth*.

The pointlike source, surrounded by diffuse emission, is centered at R.A. = $16^{\text{h}}17^{\text{m}}29.35^{\text{s}}$, decl. = $-50^{\circ}55'12.8''$. The position uncertainty is dominated by the uncertainty of the *Chandra* absolute astrometry, $0.65''$ at the 90% confidence level for sources within $2'$ from the optical axis on the ACIS-I3 chip⁷. As this position differs by only $0.62''$ from the radio position of J1617 reported by Kaspi et al. (1999), the pointlike source must be the X-ray counterpart of the radio pulsar. The amorphous diffuse emission around J1617 is distinguishable from the background up to $\approx 1'$ from the pulsar. The background-subtracted surface brightness of this

⁷ See §5.4 and Fig. 5.1 of the *Chandra* Proposers' Observatory Guide v. 10 at <http://asc.harvard.edu/proposer/POG>.

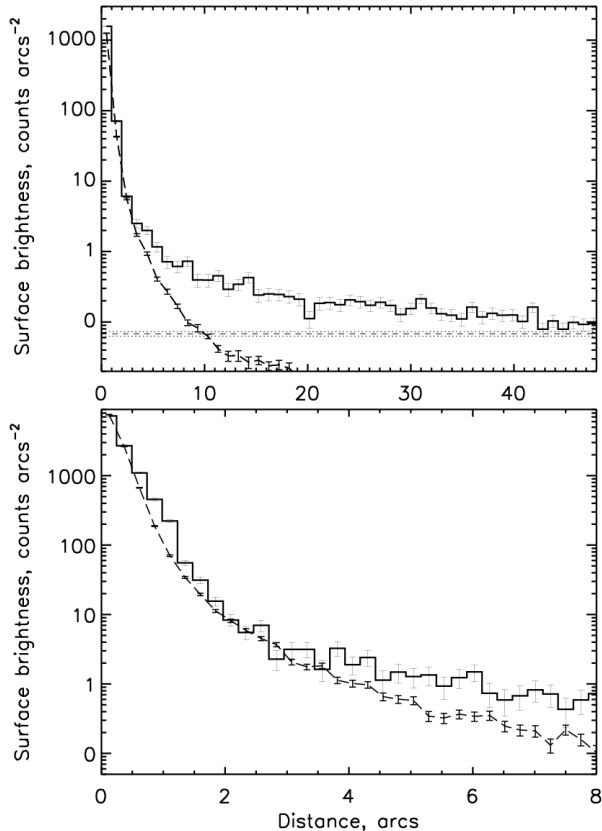


FIG. 3.— Radial profiles of the observed emission around the pulsar position and the simulated PSF in the 2–8 keV band. The histogram in the *top* panel (bin size $1''$) demonstrates the large-scale PWN emission. The histogram in the *bottom* panel (bin size $0.25''$) shows the compact inner PWN contribution, including the excess at $\approx 0.5''$ – $1.5''$ from the pulsar (see also §2.1 and Fig. 4).

extended PWN is $\simeq 0.002$ – 0.01 counts arcsec $^{-2}$ ks $^{-1}$, being somewhat brighter south and southwest of the pulsar.

The radial profile of the detected emission, centered on the pulsar position, is shown in Figure 3, together with the simulated PSF⁸ and background level. We see that the extended, faint PWN prevails over the pulsar emission at distances $\gtrsim 5''$ from the pulsar.

Given the large distance to the pulsar and the faintness of the extended PWN, one could expect a more compact PWN component, which would not be immediately seen in pipeline-processed data. To search for such a component, we produced images of the immediate pulsar vicinity at subpixel resolution (see Fig. 4). We first removed the pipeline pixel randomization and applied the sub-pixel resolution tool to split-pixel events in the image (Tsunemi et al. 2001; Mori et al. 2001). We then simulated the PSF image in the 2–8 keV energy band at the same position on the detector as in the real observation. We binned the observed image and the simulated PSF by a factor of 0.2 compared to the original ACIS pixel size. Finally, we used the CIAO ver. 4.0 implementation (provided as an `arestore` script) of the Lucy-Richardson deconvolution algorithm (Lucy 1974). We ran `arestore` with several settings for different numbers of iterations, between 30 and 200,

⁸ To simulate the PSF with ChaRT and MARX, we followed the steps outlined in <http://cxc.harvard.edu/chart/threads/index.html>. We have also tried several values of the Dither Blur parameter (see <http://cxc.harvard.edu/chart/caveats.html> and Misanovic et al. 2007 for discussion) and adopted the value of $0.1''$ that provides the best match between the simulated PSF and the real data within $r \lesssim 3''$ from the pulsar.

and noticed that the iterations converge (i.e., no new structure appear) once the number of iterations approaches 100.

Examples of such deconvolved images are shown in Figure 4 for 30, 100, and 200 iterations (panels *b*, *c*, and *d*, respectively). When the number of iterations approaches 30, the deconvolved image starts to reveal an extended structure ($\approx 2''$ in linear extent) elongated in the south-north direction, with the point source being in the middle of this structure. With increasing the number of iterations, the elongated structure becomes one-sided (i.e., it appears only to the south of the point source), and an arclike feature, roughly perpendicular to the southern elongation, appears at about $1''$ north of the pulsar. Increasing the number of iterations beyond ≈ 100 does not change the structure of the compact extended emission. The exposed features of the deconvolved images could be interpreted as a jet (south of the pulsar) and an arc (perhaps part of a ring or a torus). Note that similar features are often seen in *Chandra* images of PWNe around young pulsars (see e.g., KP08). The radial profile shown in Figure 3 (*bottom*) demonstrates the significance of the count excess at $r \approx 0.5''$ – $1.5''$ from the pulsar.

For comparison, we also show a deconvolved ACIS image without removing the pipeline pixel randomization (Fig. 4*e*). Although the deconvolution of this image does not recover as much structure as the images with the pixel randomization removed, it does show some of the features that are seen in the deconvolved non-randomized images.

To test reliability of the deconvolution procedure, we applied it to the ACIS image of the CCO in the Cas A SNR (ObsID 6690), a radio-silent NS showing no radio pulsar activity, for which no PWN is expected (e.g., Pavlov et al. 2004). The ACIS image of the CCO has ≈ 7200 counts within the $0.98''$ radius around the source, comparable to J1617 in our ACIS-I image. Unlike J1617, the deconvolved image of the Cas A CCO preserves the pointlike appearance with no extended structure (see Fig. 4*f*). Although, as any deconvolution algorithm, `arestore` could introduce artifacts in the images, the test example of the Cas A CCO provides credibility to the features seen in the deconvolved images of J1617.

2.2. The field of HESS J1616–508.

Since J1617 is considered as a plausible counterpart for the extended TeV source HESS J1616 (Landi et al. 2007), we have searched for additional data in the *Chandra* and *XMM-Newton* archives that would provide at least partial coverage of the HESS J1616 extent and allow us to look for other potential X-ray counterparts of the TeV source and examine its connection to J1617. In the *Chandra* archive we found an ACIS observation of the Kes 32 SNR (Vink 2004). During that observation, the S2 and S3 chips imaged the central part of HESS J1616 (see Fig. 5*a*). The brightest source (marked X in Fig. 5*a*) is located on the S2 chip around R.A. $\approx 16^{\text{h}} 16^{\text{m}} 10^{\text{s}}$, decl. $\approx -50^{\circ} 54' 30''$. Because of the small number of counts (140 ± 20 counts within an $r = 40''$ circle in 0.5–8 keV; $S/N \approx 7$) and the broad PSF (FWHM $\approx 15''$ at the off-axis angle $\theta \approx 16'$), it is difficult to determine whether the source is extended or multiple; however, with the linear extent of $\simeq 1'$, it does not appear to be point-like. Assuming an absorbed PL spectrum with $\Gamma = 1.5$ and $n_{\text{H},22} \equiv n_{\text{H}}/10^{22} \text{ cm}^{-2} = 3.45$ (as found from the fit to the pulsar spectrum; see §2.3.1), the unabsorbed 0.5–8 keV flux of source X can be estimated as $F_{\text{X}} \sim (1.7\text{--}2.2) \times 10^{-13} \text{ ergs cm}^{-2} \text{ s}^{-1}$.

We see some hints of extended emission southwest of source X; however, the low count rate, ~ 1.4 counts ks $^{-1}$

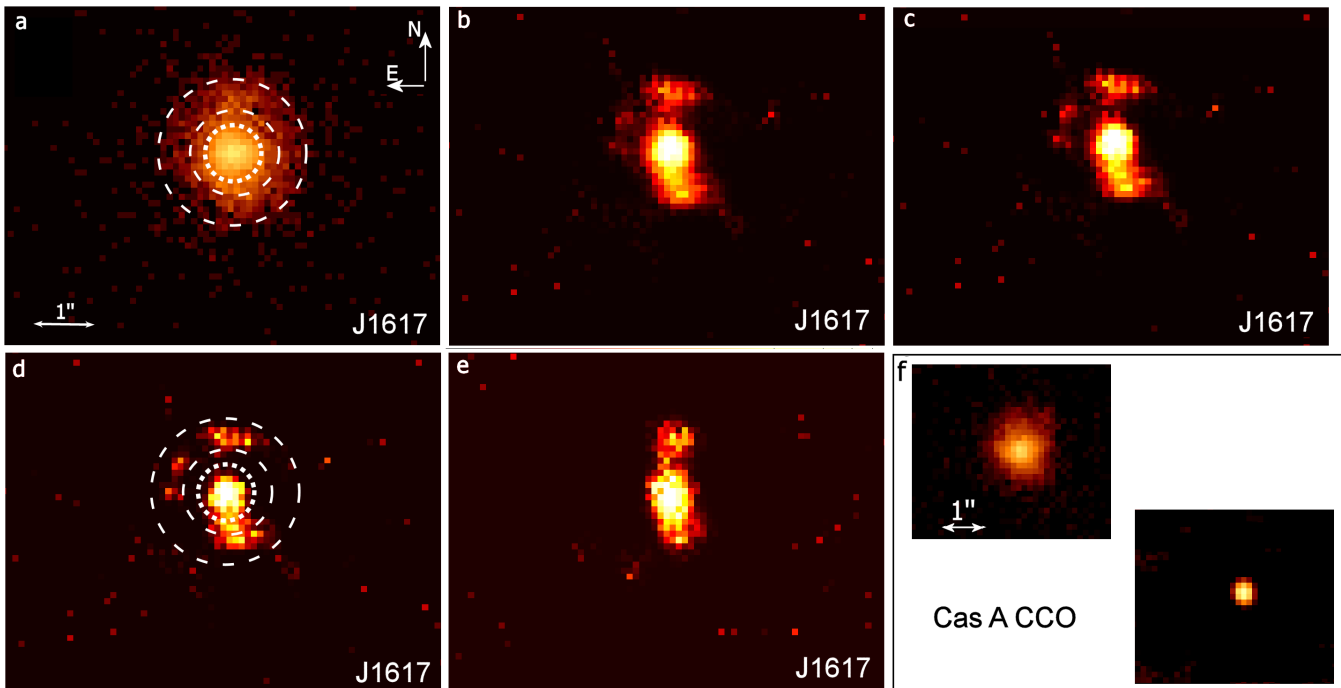


FIG. 4.— *a*: Original ACIS-I3 image of pulsar and its immediate vicinity (pixel size $0.1''$), with pipeline pixel randomization removed (circle radii are $0.5''$, $0.74''$ and $1.25''$). *b*, *c*, and *d*: Deconvolved images obtained with *arestore* from the image in panel *a* after 30, 100, and 200 iterations, respectively. *e*: Same as *c* but without removing the pipeline pixel randomization in the original image. *f*: Original (top left; pixel size $0.1''$, pipeline randomization removed) and deconvolved (bottom right; *arestore* with 100 iterations) images of the Cas A CCO. See text for details.

arcmin $^{-2}$ in 0.5–8 keV (corresponding to the unabsorbed surface brightness of $\sim 6 \times 10^{-14}$ ergs cm $^{-2}$ s $^{-1}$ arcmin $^{-2}$ for the PL model with $\Gamma = 1.5$ and $n_{\text{H},22} = 3.45$) precludes any detailed analysis of this diffuse emission.

Source X falls near the edge the EPIC FOV in the 2001 observation (Fig. 5*b*). Although some emission at the source X position is discernible, it is not possible to determine whether the source is extended or pointlike. Its brightest part in the EPIC image is shifted by about $30''$ southwest from the *Chandra* position (the difference could result from a statistical noise and background fluctuations).

Source X was outside the EPIC FOV in the 2005 *XMM-Newton* observation. Because of the low surface brightness and large XIS PSF, the source is not seen in the *Suzaku* data. Deeper ACIS or EPIC observations, with the center of the TeV source imaged close to the optical axis, are required to understand the nature of the detected extended X-ray emission.

In addition to analyzing the X-ray images, we examined the available IR and radio data on the region of interest. The 843 MHz image from the Sydney University Molonglo Sky Survey (SUMSS) shows some diffuse emission surrounding the very central part of HESS J1616 (within the innermost TeV contour shown in Fig. 5*a,f*). The radio emission looks like a patchy, elongated shell, possibly an unknown SNR (alternatively, it could be several faint point sources accidentally aligned in a shell-like structure). The *Spitzer* IRAC images of the same region (Fig. 5*e,f*) also reveal diffuse emission partly coincident with the radio emission. In addition, there are several compact sources seen in the radio and, especially, IR images within the central part of the TeV source. The brightest source, marked A in Fig. 5, is located near the TeV source center. At $8 \mu\text{m}$, source A is resolved into a complex shell with an additional lobe to the west and a number of compact point sources suggesting a star-forming region. Source X appears to have IR counterpart(s) resolved into several compact

diffuse sources at $8 \mu\text{m}$ (Fig. 5*e*), possibly also star-forming regions. Deeper radio observations with higher spatial resolution would be most helpful to understand the nature of these sources.

2.3. Pulsar timing

The data from the CC-mode observation of the RCW 103 CCO also allow one to analyze the pulsations of the J1617 pulsar since the pulsar falls within the FOV. The pulsar is clearly seen in the one-dimensional image shown in Figure 6; however, the large off-axis angle ($\approx 6'$) significantly broadens the PSF, making it impossible to separate the inner PWN and the pulsar.

For the timing analysis, we extracted 4057 photons in the 2–8 keV band from the $10''$ -wide segment centered on J1617 (shown in Fig. 6, *top*; $\approx 90\%$ of these counts are expected to come from the unresolved source, i.e., the pulsar and the compact inner PWN). The photon arrival times have been transformed to the solar system barycenter using the *axBary* tool of CIAO 3.4. We have searched for the pulsed signal near the expected radio pulsation frequency and found $Z_{1,\text{max}}^2 = 301$ (see Buccheri et al. 1983 for details on Z_n^2 statistics) at $\nu = 14.414488 \text{ Hz} \pm 1 \mu\text{Hz}$, consistent with the frequency expected from the radio ephemeris at the epoch of the *Chandra* observation. The light curve folded at this frequency reveals a single pulse with a flat minimum (see Fig. 6, *bottom*). The observed 2–8 keV pulsed fraction is $40\% \pm 4\%$. Correcting it for the background contribution (which includes the outer PWN), we obtain $44\% \pm 4\%$. The pulse profiles extracted in narrower energy bands (2–4 and 4–8 keV) are similar to the 2–8 keV pulse profile, both in shape and pulsed fraction.

2.4. Spectral analysis

2.4.1. Pulsar

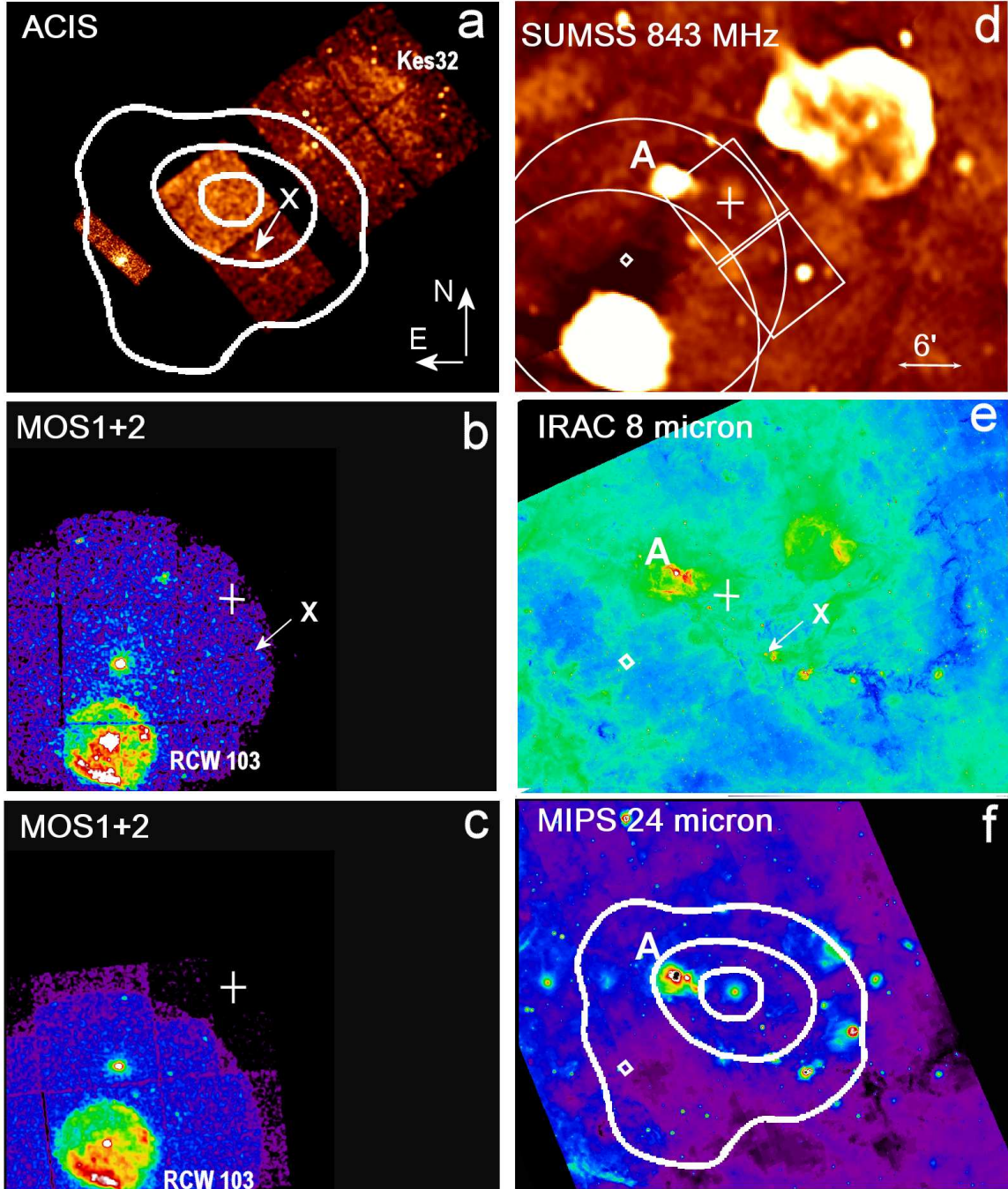


FIG. 5.— X-ray, radio and IR images of the J1617 and HESS J1616 field. *a*: Combined 0.5–8 keV image from two ACIS observations (2006 June and 2001 October) with TeV contours (from Aharonian et al. 2006) overlotted. *b* and *c*: MOS1+2 images in the 0.5–8 keV band from the *XMM-Newton* observations of 2001 September and 2005 August, respectively. The cross shows the center of HESS J1616. The rectangles show the region covered by the ACIS S2 and S3 chips in the *Chandra* observation of 2001 October, while the circles show the MOS1+2 FOV in the two *XMM-Newton* observations. The position of J1617 is shown by the diamond. *e* and *f*: *Spitzer* images of the field.

For our 1/4 subarray observation (ObsID 6684), we extracted the pulsar’s spectrum (using the CIAO’s *psextract* task) from a small circular aperture of $r = 0.5''$ to minimize the contamination from the compact PWN (see Fig. 3, *bottom*, and also Fig. 4*a,d*). No background subtraction was attempted because the PWN contribution is expected to be negligible in this small aperture (Fig. 3, *bottom*). The 2853 counts extracted from the $0.5''$ radius aperture (52% encircled energy fraction) in the 1–8 keV range (there are virtually no counts below 1 keV) correspond to the aperture-corrected source count rate of 96 ± 2 counts ks^{-1} . The corresponding

absorbed flux is $F_{\text{psr}} \simeq 2.15 \times 10^{-12}$ ergs cm^{-2} s^{-1} . With the (exposure) frame time of 0.8 s, the expected pile-up fraction is very small ($\approx 3\%$ according to PIMMS⁹).

We binned the spectrum with minimum of 50 counts per bin and fit the absorbed PL model in the 1–8 keV range with all the fitting parameters allowed to vary. The quality of the fit is excellent ($\chi^2_{\nu} = 1.04$ for 49 degrees of freedom [dof]; see Fig. 7). The hydrogen column density, $n_{\text{H},22} = 3.45 \pm 0.14$ (see Fig. 8; the errors here and below are at the 68% confidence level for a single interesting parameter) is a factor of

⁹ <http://cxc.harvard.edu/toolkit/pimms.jsp>

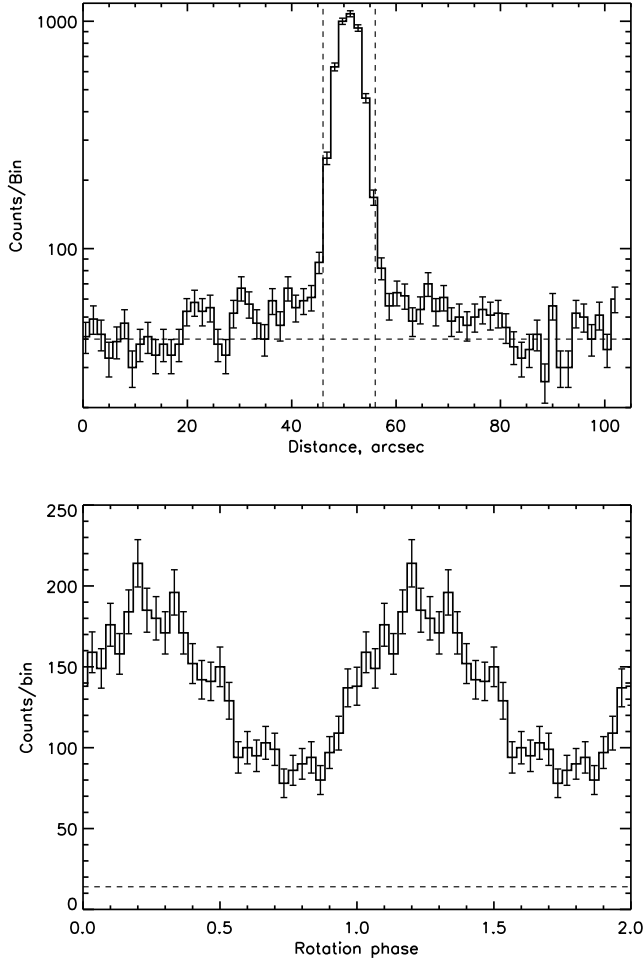


FIG. 6.— Results from the CC-mode observation. *Top*: One-dimensional profile showing J1617 and the outer PWN above the horizontal dashed line that corresponds to the background level. The two vertical lines show the aperture from which the spectrum and the light curve were extracted. *Bottom*: The light curve with 30 phase bins. The dashed line shows the background level (including the contribution of the outer PWN).

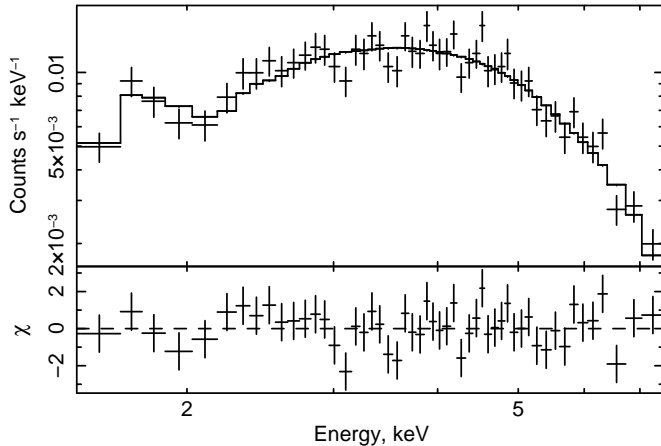


FIG. 7.— Spectrum of the pulsar in observation 6684 fitted with the PL model (see Table 3 for the fitting parameters).

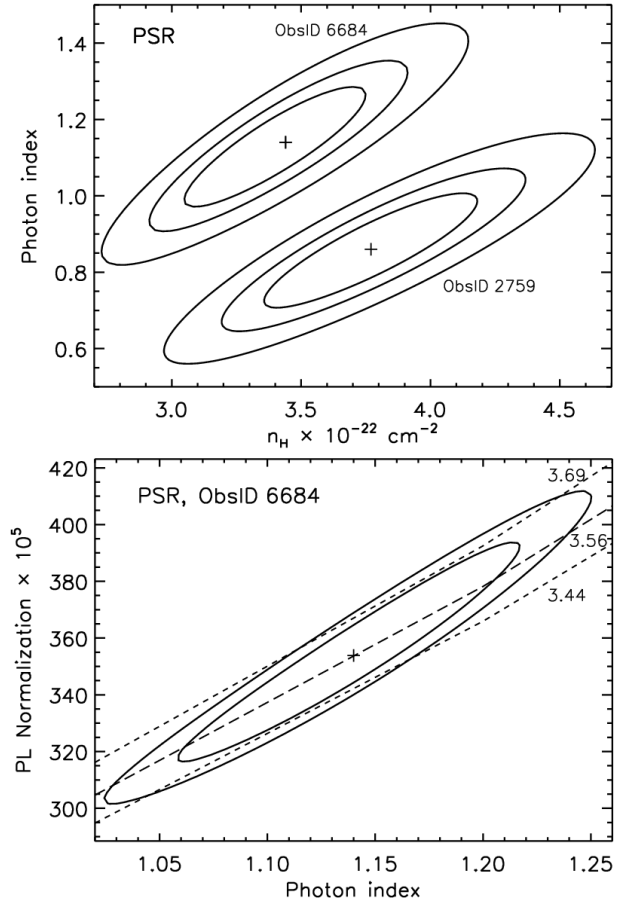


FIG. 8.— *Top*: Confidence contours (68%, 90%, and 99%) in the n_H - Γ plane for the PL fit to the pulsar spectrum from two ACIS observations (see Table 1). The contours are obtained with the PL normalization fitted at each point of the grid. *Bottom*: Confidence contours (68% and 90%) for the PL fit to the pulsar spectrum for fixed $n_{H,22} = 3.45$. The PL normalization is in units of 10^{-5} photons $\text{cm}^{-2} \text{ s}^{-1} \text{ keV}^{-1}$ at 1 keV. The dashed curves are the loci of constant unabsorbed flux in the 0.5–8 keV band; the flux values near the curves are in units of 10^{-12} ergs $\text{cm}^{-2} \text{ s}^{-1}$.

1.5 larger than the average Galactic HI column density in the direction of the pulsar ($l = 332.50^\circ$, $b = -0.28^\circ$, $n_{\text{HI},22} = 2.26$ (Dickey & Lockman 1990). This is not surprising since the n_H deduced from an X-ray spectrum under the assumption of standard element abundances generally exceeds the n_{HI} measured from 21 cm observations by a factor of 1.5–3 (e.g., Baumgartner & Mushotzky 2005). The same PL fit gives the photon index $\Gamma_{\text{psr}} = 1.14 \pm 0.06$ and the unabsorbed flux $F_{\text{psr}}^{\text{unabs}} = (3.6 \pm 0.1) \times 10^{-12}$ ergs $\text{cm}^{-2} \text{ s}^{-1}$ in the 0.5–8.0 keV band. It corresponds to the isotropic luminosity $L_{\text{psr}} \approx 1.8 \times 10^{34} d_{6.5}^2$ ergs s^{-1} ($= 1.1 \times 10^{-3} d_{6.5}^2 \dot{E}$), where $d_{6.5} = d/6.5 \text{ kpc}$ is the distance to the pulsar estimated from the dispersion measure $\text{DM} = 467 \text{ cm}^{-3} \text{ pc}$ and the Galactic electron density distribution model by Taylor & Cordes (1993)¹⁰.

We have also extracted the pulsar spectrum from the ObsID 2957 data taken in the CC mode, using the same region ($10''$ -wide segment) as for the light curve (see §2.3), which contains 4522 counts in the 1–8 keV band. Note that in this

¹⁰ The more recent model by Cordes & Lazio (2002) gives a slightly larger distance of 6.8 kpc. We caution, however, that distances based on such models are not very certain. For instance, HI absorption measurements give $\sim 20\%$ – 30% smaller distances than the Taylor & Cordes model for two pulsars within 20° of J1617 (Kaspi et al. 1998).

TABLE 3
PL FITS TO THE PULSAR AND PWN SPECTRA.

Region	$n_{\text{H},22}^{\text{a}}$	$\mathcal{N}_{-5}^{\text{b}}$	Γ	χ^2/dof	$L_{\text{X},33}^{\text{c}}$	L_{-16}^{d}
Pulsar	3.45 ± 0.14	$35.4_{-4.8}^{+7.3}$	1.14 ± 0.06	51.0/49	17.92 ± 0.07	...
Inner PWN	[3.45]	$4.2_{-1.4}^{+1.0}$	1.47 ± 0.24	17.5/19	$1.49_{-0.23}^{+0.28}$	940 ± 160
Outer PWN	[3.45]	$5.8_{-1.4}^{+1.7}$	1.65 ± 0.20	12.9/15	1.71 ± 0.25	1.3 ± 0.2

NOTE. — The uncertainties are given at the 68% confidence level for one interesting parameter. Systematic uncertainties are not included. The normalization and luminosity of the pulsar are corrected for the finite extraction aperture.

^a $n_{\text{H},22} \equiv n_{\text{H}}/10^{22} \text{ cm}^{-2}$ was fixed in the PWN fits.

^b Spectral flux in units of $10^{-5} \text{ photons cm}^{-2} \text{ s}^{-1} \text{ keV}^{-1}$ at 1 keV.

^c Isotropic luminosity in units of $10^{33} \text{ ergs s}^{-1}$ in the 0.5–8 keV band, for $d = 6.5 \text{ kpc}$.

^d Mean unabsorbed intensity in units of $10^{-16} \text{ ergs s}^{-1} \text{ cm}^{-2} \text{ arcsec}^{-2}$ in the 0.5–8 keV band.

case the extraction region is much larger than that used for ObsID 6684 because the broad off-axis PSF. The background was taken from a nearby ($1.4' - 2.4'$ from the pulsar) region located on the same chip (S2). The background contribution is $\approx 8\%$ in the 1–8 keV band. The absorbed PL fit gives $\Gamma \simeq 0.85$ and $n_{\text{H},22} \simeq 3.8$ (see Fig. 8 for the statistical uncertainties). Although the difference between the Γ values from ObsID 6684 and ObsID 2957 appears to be statistically significant, the CC-mode fit is likely less reliable because of larger unaccounted systematic uncertainties (the CTI, gain, and ACIS filter contamination corrections are less accurate in the CC mode); therefore, below we will use the more reliable spectral parameters inferred from the ObsID 6684 data.

2.4.2. PWN

We used the ObsID 6684 data to extract the PWN spectra from two regions. The brightest *inner* component is extracted from the $0.75'' < r < 1.25''$ annulus with the area of 3.14 arcsec^2 (see Fig. 4). In this case we used the pulsar spectrum as the background spectrum, after scaling the normalization according to the simulated PSF shown in Figure 3 (*bottom*). The fainter *outer* component is extracted from a polygon region (see Fig. 2) with an area of 2600 arcsec^2 (excluding the $r = 9''$ circle around the pulsar). The background was taken from the $40'' \times 65''$ box shown in Figure 2 (*top*).

The annulus region of the inner PWN component has 1162 counts (see Table 2 for details), with $\approx 63\%$ of them coming from the pulsar (treated as a background). The corresponding absorbed flux is $F_{\text{inner}} = (1.6 \pm 0.3) \times 10^{-13} \text{ ergs cm}^{-2} \text{ s}^{-1}$ in the 0.5–8 keV band. The outer PWN region contains 959 counts (54% coming from the source); its absorbed flux is $F_{\text{outer}} = (1.7 \pm 0.1) \times 10^{-13} \text{ ergs cm}^{-2} \text{ s}^{-1}$ in the same band.

We binned the spectra extracted from the inner and outer regions with a minimum of 50 counts per spectral bin. We then fit the spectra with the absorbed PL model with the hydrogen column density fixed at the best-fit value obtained from the PL fit to the pulsar spectrum, $n_{\text{H},22} = 3.45$. For the outer PWN component, we restrict the energy range to 2–8 keV because of the large contribution of the non-uniform background¹¹ at lower energies (the background contribution decreases from 46% in 0.5–8 keV to 36% in the 2–8 keV band). We find that the PL model provides a good description of the extracted spectra for both the inner and outer PWN. The pho-

¹¹ Investigation of the background spectrum shows that it has a soft component likely originating from a dust-scattering halo around the X-ray bright RCW 103.

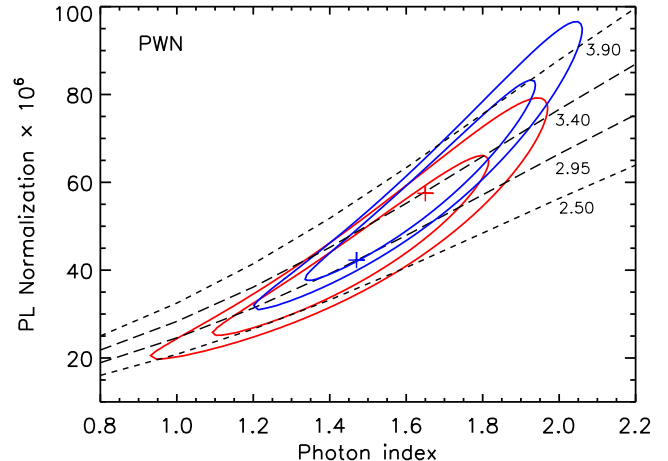


FIG. 9.— Confidence contours (68% and 90%) for the PL fit to the inner and outer PWN regions (red and blue contours, respectively; see text for the region definitions) for fixed $n_{\text{H},22} = 3.45$. The PL normalization is in units of $10^{-6} \text{ photons cm}^{-2} \text{ s}^{-1} \text{ keV}^{-1}$ at 1 keV. The dashed curves are the loci of constant unabsorbed flux in the 0.5–8 keV band; the flux values near the curves are in units of $10^{-13} \text{ ergs cm}^{-2} \text{ s}^{-1}$.

ton indices are $\Gamma_{\text{inner}} = 1.47 \pm 0.24$ and $\Gamma_{\text{outer}} = 1.65 \pm 0.20$ (see Fig. 9). Thus, the PWN spectra are noticeably softer than the pulsar spectrum. The combined unabsorbed luminosity from the two PWN regions is $L_{\text{pwn}} \approx 3.2 \times 10^{33} d_{6.5}^2 \text{ ergs s}^{-1}$ in the 0.5–8 keV band (see Table 3 for details).

3. DISCUSSION

In our high-resolution *Chandra* ACIS observation, we discovered the X-ray PWN around the young, energetic pulsar J1617. Below we discuss the pulsar and PWN properties compare them with those of other young pulsars, and discuss the connection between J1617 and the nearby HESS J1616.

3.1. Pulsar

The X-ray luminosity of J1617 is $\sim 15\%$ lower than that reported by BA02 from the *XMM-Newton* observations. The discrepancy is not surprising because the broader PSF of *XMM-Newton* includes both the pulsar and PWN contributions. Once these components are added together, the *Chandra* and *XMM-Newton* flux (and spectral slope) measurements are in agreement within their uncertainties. The 44% pulsed fraction measured from the CC-mode data is somewhat lower than that reported by BA02. The unabsorbed contribution from the inner PWN, resolved in the deconvolved images (see Figs. 3 and 4), is $\approx 10\% - 15\%$, resulting in the intrinsic pulsar's pulsed fraction of $\approx 50\%$.

The X-ray efficiency of the J1617 pulsar, $\eta_{\text{psr}} \equiv L_{\text{psr}}/\dot{E} \approx 1.1 \times 10^{-3} d_{6.5}^2$ in the 0.5–8 keV band, is typical among young pulsars (see Fig. 10, *top*). However, the spectrum of J1617 is surprisingly hard, $\Gamma_{\text{psr}} \approx 1.1$. Very few pulsars (J1509–58, J1420–6048, J1846–0258) possibly exhibit similarly hard X-ray spectra (KP08 and references therein), but the accuracies of the spectral slope measurements in these pulsars are lower than in J1617. The fact that the energy spectrum of the pulsar magnetospheric X-ray emission can be so hard has important implications for the pulsar emission models. For instance, the models that interpret the non-thermal X-ray emission as synchrotron emission from the particles produced in a pair cascade predict $1.5 < \Gamma < 2$ (e.g., Cheng et al. 1998; Crusius-Wätzel et al. 2001), i.e. softer than the spectrum we measured.

On the other hand, the so-called “full polar cap cascade” models, in which the X-rays are produced by the resonant inverse Compton scattering of the thermal emission from the hot NS surface (Zhang & Harding 2000), can explain harder spectra, with $\Gamma_{\text{psr}} \simeq 1$ (Fang & Zhang 2006). Hard spectra ($\Gamma \simeq 2/3$) are possible in the models with curvature-radiation-induced cascades in which curvature radiation may dominate synchrotron radiation even below ~ 10 keV (Rudak & Dyks 1999), although this emission mechanism is more commonly considered for higher energies. Finally, a hard spectrum could be produced via the resonant inverse Compton scattering of the radio photons if this process contributes substantially to the X-ray band (Petrova 2008). Measurements at higher energies with *Integral* and *RXTE* suggest a mild softening of the pulsar spectrum, by $\Delta\Gamma \approx 0.2\text{--}0.3$ (see Fig. 5 in Landi et al. 2007). Such behavior is opposite to the spectral hardening observed in magnetars, which is attributed to comptonization of the thermal emission from the NS surface by the relativistic electrons in the NS magnetosphere (Fernández & Thompson 2007; Baring & Harding 2008).

The lack of thermal component in the detected pulsar emission might be explained by its intrinsic faintness relative to the strong magnetospheric emission in this young pulsar. However, it is hard to constrain its contribution because, at $n_{\text{H},22} \approx 3.5$, the soft thermal X-rays are strongly absorbed by the ISM.

3.2. PWN

Unlike the pulsar, the X-ray efficiency of the J1617 PWN (compact + extended), $\eta_{\text{pwn}} \equiv L_{\text{pwn}}/\dot{E} = 2 \times 10^{-4} d_{6.5}^2$ in the 0.5–8 keV band, is noticeably lower than those of other young PWNe (Fig. 10, *middle*), except for J1357–6429 (Zavlin 2007). Also, the ratio of the PWN to pulsar luminosities, $L_{\text{pwn}}/L_{\text{psr}} \approx 0.18$ (independent of the poorly known distance), is among the lowest (Fig. 10, *bottom*), and it is significantly lower than the average $L_{\text{pwn}}/L_{\text{psr}} \sim 4$ reported by Kargaltsev et al. (2007a) and KP08. The actual PWN efficiency and the $L_{\text{pwn}}/L_{\text{psr}}$ value could be higher for J1617 (and J1357–6429) if the compact PWN component is not completely resolved from the pulsar. An upper limit on the luminosity of the unresolved PWN core follows from the timing analysis (see §2.3 and §3.1). The luminosity of the unresolved core cannot exceed $\approx 50\%$ of the pulsar luminosity (assuming that the pulsar emission is 100% pulsed), which still leaves the J1617 PWN underluminous compared to majority of PWNe (see Fig. 10 and the discussion below).

KP08 found that the X-ray efficiencies of PWNe show a very large scatter, $\eta_{\text{pwn}} \sim 10^{-5}\text{--}10^{-1}$. The cause of such a large scatter is still not understood. One could attribute the scatter to environmental differences (e.g., ISM pressure and density); however, the surprisingly good correlation between the PWN luminosities and non-thermal pulsar luminosities (with a much smaller scatter, $0.1 \lesssim L_{\text{pwn}}/L_{\text{psr}} \lesssim 10$; KP08) calls for a different explanation because L_{psr} does not depend on the environment.

The deconvolved *Chandra* images of J1617 suggest a compact structure at a distance of $\sim 1''$ ($= 9.7 \times 10^{16} d_{6.5}$ cm) from the pulsar (see Fig. 4), which could be a torus beyond the termination shock in the pulsar wind. Assuming that the ram pressure caused by the pulsar motion is lower than the ambient pressure, we can estimate the latter as

$$p_{\text{amb}} \sim \dot{E} f_{\Omega} (4\pi r_s^2)^{-1} \quad (1)$$

where r_s is the termination shock radius in the equatorial

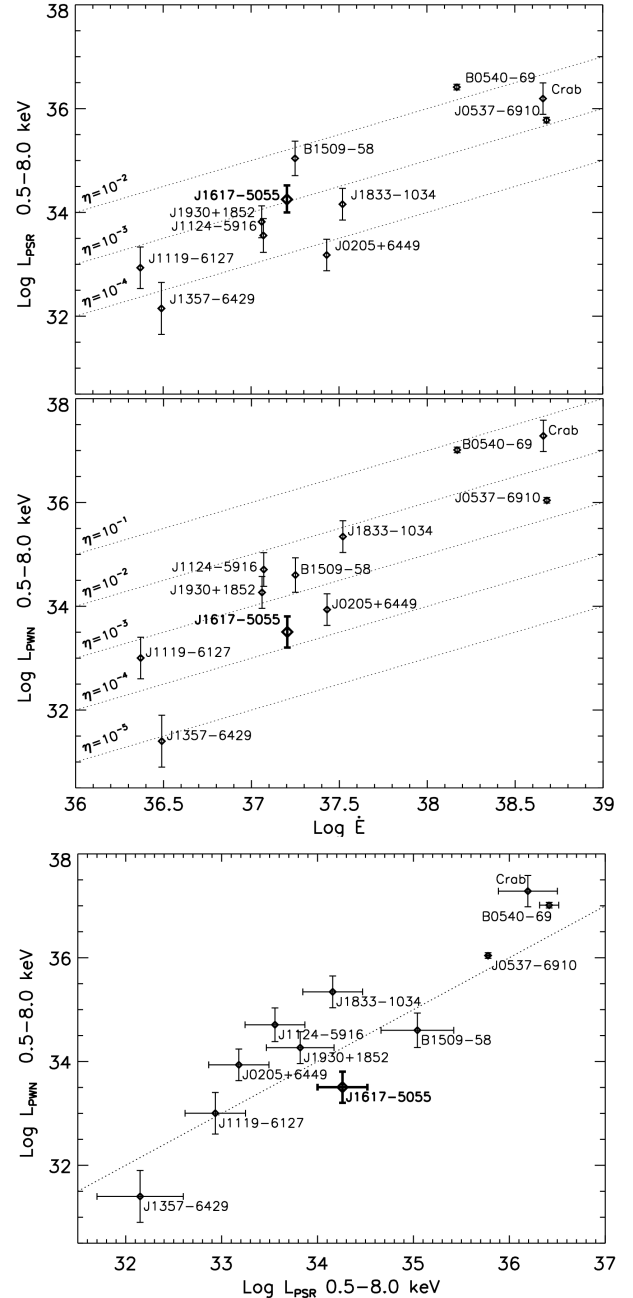


FIG. 10.— *Top*: Pulsar luminosity vs. spin-down power \dot{E} . *Middle*: PWN luminosity vs. \dot{E} . *Bottom*: Pulsar luminosity vs. PWN luminosity. The top and middle panels show the lines of constant X-ray efficiency, while the dashed line in the bottom panel corresponds to $L_{\text{psr}} = L_{\text{pwn}}$. (Based on the data published by KP08.)

plane, and the factor f_{Ω} takes into account possible anisotropy of the pulsar wind. For J1617, this estimate gives $p_{\text{amb}} \sim 1.7 \times 10^{-8} f_{\Omega} (r_s/5 \times 10^{16} \text{ cm})^{-2} \text{ ergs cm}^{-3}$. It is unlikely that the X-ray PWN is more compact than it follows from our image analysis (which would imply that the true PWN luminosity and its ratio to L_{psr} are higher than estimated above) because the inferred pressure is already quite high (cf. Table 2 in Kargaltsev et al. 2007a). Therefore, we suggest that in some PWNe, including J1617, the radiative efficiency of the shocked pulsar wind is well below the average. The low PWN luminosity cannot be attributed to inefficient pair production in the pulsar magnetosphere because the non-thermal pulsar luminosity is close to its typical value. However, the faintness

of the PWN could be attributed to inefficient particle acceleration on the way to (or at) the termination shock. The physical mechanism responsible for particle acceleration is currently unknown, and the processes occurring upstream of the shock are poorly understood (Arons 2007; Kirk et al. 2007). We can only speculate that these processes may depend of the angle between the pulsar magnetic and rotation axes (e.g., a larger misalignment of the axes may lead to faster conversion of the magnetic field energy to the particle energy via more efficient reconnection). They may also depend on the termination shock radius, which, in turn, depends on the ambient pressure. For instance, if r_s is small, there may not be enough time for the dissipative processes to convert the magnetic field energy to the particle energy (e.g., Arons 2008). Yet, even in this case, most of the pulsar’s rotational energy is being lost as a wind, but the wind may have a higher magnetization parameter and lower particle energies (see, e.g., Arons 2007 for a pulsar wind theory review) than in the case of X-ray bright PWNe. A higher-than-typical ambient pressure (hence a small termination shock radius) is plausible because the young pulsar should be within the host SNR interior (which remains undetected because of the strong X-ray absorption). The wind still should emit synchrotron radiation downstream of the termination shock but possibly at lower frequencies as the characteristic synchrotron frequency is proportional to the electron Lorentz factor squared. Unfortunately, observing at lower X-ray energies or in the optical is impossible because of the strong ISM absorption, but sensitive far-IR and radio observations would be useful.

3.3. Connection to HESS J1616–508

J1617 is located $\sim 10'$ east of the TeV source HESS J1616–508 (see Fig. 5). Despite the large offset, the young, energetic pulsar is still within the TeV source extent, and it has been considered as a plausible candidate for powering the TeV emission (Aharonian et al. 2006; Landi et al. 2007), mainly based on energetics arguments ($L_{\text{TeV}} \sim 10^{-2}\dot{E}$). Extended TeV sources have recently been discovered in the vicinity of a few (≈ 15) young pulsars, leading to the suggestion that the TeV emission comes from *relic PWNe* crushed by the asymmetric SNR reverse shock that arrived to the pulsar location a few kys ago (e.g., de Jager 2006; Kargaltsev et al. 2007b; Kargaltsev & Pavlov 2007). The original model developed by Blondin et al. (2001) suggests that the synchrotron emitting electrons from the pulsar wind can be swept up by the asymmetric reverse shock to one side of the pulsar. The resulting “offset PWNe” will contain aged electrons that still can produce observable radio synchrotron emission as well as high-energy γ -ray emission via the inverse Compton scattering of background photons by relativistic electrons.

The high-resolution ACIS observations of J1617 do not reveal a preferential extension of the J1617 PWN towards the TeV source (rather there is a hint of extension in the opposite

direction; see §2.1 and Fig. 1), such as observed in some other TeV sources neighboring young pulsars (Kargaltsev & Pavlov 2007; Pavlov et al. 2008). Therefore, we conclude that there is no convincing evidence linking the TeV source to J1617.

The HESS J1616 field has been observed with several X-ray missions. The *XMM-Newton* and *Suzaku* images do not reveal any X-ray sources within the TeV bright part of HESS J1616, making it one of the best examples of a “dark accelerator” (Matsumoto et al. 2007). Yet, the examination of the 30 ks ACIS image covering the central part of the HESS J1616 field, reveals the possibly extended source X (see Fig. 5 and §2.2). This source, however, has a very low X-ray flux resulting in a surprisingly small $L_X/L_{\text{TeV}} = (1-2) \times 10^{-3}$ (cf. Table 2 in Kargaltsev et al. 2007b). Furthermore, the radio and IR images shown in Figure 5 reveal some diffuse emission and pointlike sources within the central part of HESS J1616. The diffuse emission resembles a shell, while one of the bright IR pointlike sources coincides with the center of the TeV source. Therefore, we speculate that HESS J1616 may consist of two (or more) unresolved sources, one of which might be associated with J1716, while the other(s) could be associated with the extended radio/IR emission (possibly an SNR or a star-forming region). Deeper radio and X-ray observations or TeV observations with higher resolution can test this hypothesis.

4. SUMMARY

We have discovered a surprisingly underluminous PWN around the young, energetic pulsar J1617. The PWN consists of a compact and extended components of comparable luminosities. The faintness of the PWN could be attributed to the intrinsically low radiative efficiency of the pulsar wind. We have also obtained an accurate measurement of the pulsar’s X-ray spectrum, which fits an absorbed PL with $\Gamma_{\text{psr}} \approx 1.1$, harder than predicted by the models of synchrotron emission from relativistic electrons/positrons produced in the pair-cascade.

J1617 has been considered as a plausible counterpart to the offset TeV source HESS J1616; however, the X-ray PWN does not show any asymmetry towards HESS J1616. On the other hand, the archival X-ray, IR, and radio data that cover the central region of HESS J1616 reveal some diffuse emission, allowing for alternative interpretations of the TeV emission.

Support for this work was provided by the National Aeronautics and Space Administration through Chandra Award Number GO6-7051X issued by the Chandra X-ray Observatory Center, which is operated by the Smithsonian Astrophysical Observatory for and on behalf of the National Aeronautics Space Administration under contract NAS8-03060

REFERENCES

- Aharonian, F., et al. 2006, *ApJ*, 636, 777
Aoki, T., Dotani, T., & Mitsuda, K. 1992, *IAUC* 5588
Arons, J. 2007, in *Proc. 363rd W. E. Heraeus Seminar on Neutron Stars and Pulsars*, eds. W. Becker & H. H. Huang (Munich: MPE Report No. 291) (astro-ph/0708.1050)
Arons, J. 2008, in *40 Years of Pulsars: Millisecond Pulsars, Magnetars, and More*, eds. C. Bassa, A. Cumming, V. M. Kaspi, & Z. Wang, *ASP Conf. Proc.*, 983, 200 (preprint arXiv:0710.5261)
Baumgartner, W. H., & Mushotzky, R. F. 2006, *ApJ*, 639, 929
Baring, M. G. & Harding, A. K. 2008, in *Astrophysics of Compact Objects*, *AIP Conf. Proc.*, 968, 93
Becker, W., & Aschenbach, B., 2002, *Proc. of 270th WE-Heraeus Seminar on Neutron Stars, Pulsars and Supernova Remnants*, eds. W. Becker, H. Lesch & J. Trümper, *MPE Report*, p. 64 (BA02)
Blondin, J., Chevalier, R., & Frierson, D. 2001, *ApJ*, 563, 806
Buccheri, B., et al. 1983, *A&A*, 128, 245
Cheng, K. S., Gil, J., & Zhang, L. 1998, *ApJ*, 493, L35
Cordes, J. M., & Lazio, T. J. W. 2002, preprint (arXiv:astro-ph/0207156)
Crusius-Wätzell, A. R., Kunzl, T., & Lesch, H. 2001, *ApJ*, 546, 401

- de Jager, O. 2006, 26th IAU Meeting, On the Present and Future of Pulsar Astronomy, Joint Discussion 2, 16-17 August, 2006, Prague, Czech Republic, JD02, #53
- de Luca, A., Caraveo, P. A., Mereghetti, S., Tiengo, A., & Bignami, G. F. 2007, *Ap&SS*, 308, 231
- Dickey, J. M., & Lockman, F. J. 1990, *ARA&A*, 28, 215
- Fang, J. & Zhang, L. 2006, *ApJ*, 653, 573
- Fernández, R., & Thompson, C. 2007, *ApJ*, 660, 615
- Gaensler, B. M., & Slane, P. O. 2006, *ARA&A*, 44, 17
- Garmire, G. P., Garmire, A. B., Burrows, D. N., & Pavlov, G. G. 1999, *BAAS*, 31, 1427
- Gotthelf, E. V., Petre, R., & Hwang, U. 1997, *ApJ*, 487, L175
- Kargaltsev, O. & Pavlov, G. G. 2007, *ApJ*, 670, 655
- Kargaltsev, O., & Pavlov, G. G. 2008, in 40 Years of Pulsars: Millisecond Pulsars, Magnetars, and More, eds. C. Bassa, A. Cumming, V. M. Kaspi, & Z. Wang, ASP Conf. Proc., 983, 171 (preprint arXiv0801.2602) (KP08)
- Kargaltsev, O., Pavlov, G. G., & Garmire, G. P. 2007a, *ApJ*, 660, 1413
- Kargaltsev, O., Pavlov, G. G., & Garmire, G. P. 2007b, *ApJ*, 670, 643
- Kaspi, V. M., Crawford, F., Manchester, R. N., et al. 1998, *ApJ*, 503, L161
- Kaspi, V. M., Roberts, M. S. E., & Harding, A. K. 2006, in Compact Stellar X-ray Sources, ed. W. H. G. Lewin & M. van der Klis (Cambridge: Cambridge Univ. Press), 279
- Kirk, J. G., Lyubarsky, Y., & Petri, J. 2007, in Proc. 363rd W. E. Heraeus Seminar on Neutron Stars and Pulsars, eds. W. Becker & H. H. Huang (Munich: MPE Report No. 291) (preprint astro-ph/0703116)
- Kuiper, L. 2007, in Multifrequency behaviour of high-energy cosmic sources, May 28 – June 2, Vulcano, Italy, (http://workshop2007.iasf-roma.inaf.it/talks/thursday_morning_kuiper.pdf)
- Landi, R., De Rosa, A., Dean, A. J., Bassani, L., Ubertini, P., & Bird, A. J. 2007, *MNRAS*, 380, 926
- Lucy, L. B. 1974, *AJ*, 79, 745
- Matsumoto, H., et al. 2007, *PASJ*, 59, 151
- Misanovic, Z., Pavlov, G. G., & Garmire, G. P. 2007, *ApJ*, submitted (preprint arXiv:0711.4171)
- Mori, K., Tsunemi, H., Miyata, E., Baluta, C., Burrows, D. N., Garmire, G. P., & Chartas, G. 2001, in New Century of X-ray Astronomy, ASP Conf. Proc. Vol. 251. Ed. H. Inoue & H. Kunieda (San Francisco: ASP), 576
- Pavlov, G. G., Sanwal, D., Garmire, G. P., & Zavlin, V. E. 2002, in Neutron Stars in Supernova Remnants, eds. P. O. Slane & B. M. Gaensler, ASP Conf. Ser., 271, 247
- Pavlov, G. G., Sanwal, D., & Teter, M. A. 2004, in IAU Symp. 218, Young Neutron Stars and Their Environments, eds. F. Camilo & B. M. Gaensler (San Francisco: ASP), 239 (preprint astro-ph/0311526)
- Pavlov, G. G., Kargaltsev, O., & Briskin, W. F. 2008, *ApJ*, 675, 683
- Petrova, S. A. 2008, *MNRAS*, 383, 1413
- Rudak, B. & Dyks, J. 1999, *MNRAS*, 303, 477
- Taylor, J. H., & Cordes, J. M. 1993, *ApJ*, 411, 674
- Torii, K., et al. 1998, *ApJ*, 494, L207
- Torii, K., Gotthelf, E. V., Vasisht, G., Dotani, T., & Kinugasa, K. 2000, *ApJ*, 534, L71
- Tsunemi, H., Mori, K., Miyata, E., Baluta, C., Burrows, D. N., Garmire, G. P., & Chartas, G. 2001, *ApJ*, 554, 496
- Vink, J. 2004, *ApJ*, 604, 693
- Zavlin, V. E. 2007, *ApJ*, 665, 143
- Zhang, B. & Harding, A. K. 2000, *ApJ*, 532, 1150